PAPER

Constraints on cosmic-ray boosted dark matter with realistic cross section

To cite this article: Atanu Guha and Jong-Chul Park JCAP07(2024)074

View the article online for updates and enhancements.

Constraints on cosmic-ray boosted dark matter with realistic cross section

Atanu Guha [iD] **and Jong-Chul Park** [iD]

Department of Physics and Institute of Quantum Systems,
Chungnam National University,
Daejeon, 34134, Republic of Korea

E-mail: atanu@cnu.ac.kr, jcpark@cnu.ac.kr

ABSTRACT: Sub-MeV cold dark-matter particles are unable to produce electronic recoil in conventional dark-matter direct detection experiments such as XENONnT and LUX-ZEPLIN above the detector threshold. The mechanism of boosted dark matter comes into picture to constrain the parameter space of such low mass dark matter from direct detection experiments. We consider the effect of the leading components of cosmic rays to boost the cold dark matter, which results in significant improvements on the exclusion limits compared to the existing ones. To present concrete study results, we choose to work on models consisting of a dark-matter particle χ with an additional $U(1)'$ gauge symmetry including the secluded dark photon, $U(1)_{B-L}$, and $U(1)_{L_e-L_\mu}$. We find that the energy dependence of the scattering cross section plays a crucial role in improving the constraints. In addition, we systematically estimate the Earth shielding effect on boosted dark matter in losing energy while traveling to the underground detector through the Earth.

JCAP07(2024)074

Contents

1 Introduction

Various astrophysical evidences strongly support the notion of the existence of large amount of dark matter (DM) in our Universe [1, 2]. Even though primary indication comes only from the gravitational effects, efforts have been made to extract some information about the interaction between DM particles and standard model (SM) particles. One of the most promising avenues is to observe the recoil spectrum of SM targets when DM particles scatter off them [3]. This idea has been implemented in the leading direct detection experiments [4–10].

The most stringent constraint on the spin-independent elastic scattering cross section of cold DM with nucleon is now given as $\sim 5 \times 10^{-48}\,\mathrm{cm}^2$ at $30\,\mathrm{GeV}$ of DM mass [11]. The strongest limit on DM-electron elastic scattering cross section is given by $\sim 5 \times 10^{-41}\,\mathrm{cm}^2$ at $200\,\mathrm{MeV}$ of DM mass [12]. Direct detection experiments lose sensitivity for DM with low mass as energy transfer is less efficient for the lighter cold DM to overcome their detection threshold energies. The lowest mass explored by direct detection experiments till date is

$\sim 0.5\,\mathrm{MeV}$ when DM-electron interaction is considered [13–16], while $\sim 0.2\,\mathrm{GeV}$ when DM-nucleon spin-independent interaction is considered [17]. In our solar neighbourhood, the average velocity of halo DM is approximately 10^{-3} of the speed of light which is the primary cause for the low mass cold DM to fail to induce recoils above the detector threshold energy. Quantitatively, the XENONnT experiment loses sensitivities for sub-GeV DM in case of nuclear recoils and for sub-MeV DM in case of electron recoils.

To overcome this difficulty, various classes of boosted dark matter (BDM) have been proposed in literature.[1] Among them, two component DM models with a hierarchical mass spectrum [24–39], charged cosmic-ray boosted DM (CRBDM) [40–54], and cosmic-ray neutrino BDM (νBDM) [55–59] have received special attention in recent times. Moreover, numerous phenomenological studies of BDM motivated several neutrino and DM experiments to study and report dedicated search results of BDM [60–64]. We consider the effect of the leading components of cosmic rays [65, 66] to boost the cold DM, and find that there is significant improvements on the exclusion limits compared to the existing literature.

Working with the energy independent constant cross section for the whole mass range of DM provides a rough estimation about the exclusion region in the DM mass vs DM-SM interacting cross section parameter space [50]. However, to present a concrete example, we choose to work on models described below consisting of a Dirac fermion χ with a new U(1)$'$ gauge symmetry. In the secluded dark photon model [67–69], the new gauge boson A' is kinetically mixed with the SM U(1) gauge boson and that is how DM can interact with SM particles through the vector portal. Whereas, for another model we explored, namely, U(1)$_{B-L}$, the new U(1)$'$ gauge symmetry stands for the conservation of the difference between the baryon number and the lepton number. DM fermions are assumed to be charged under the U(1)$_{B-L}$ symmetry, while SM fermions are charged under U(1)$_{B-L}$ for obvious reason. Similar logic holds for the U(1)$_{L_e - L_\mu}$ model where the new U(1)$'$ gauge symmetry stands for the conservation of the difference between the electronic lepton number and the muonic lepton number. All of the models stated above are capable of depicting DM-SM interactions through the new U(1)$'$ gauge boson as the mediator.[2] We will work on the above mentioned benchmark models and show that the energy dependence of the cross section plays a crucial role in improving the constraints.

We organize the subsequent discussion as follows. In section 2, we briefly summarize the leading components of cosmic ray and estimate the corresponding fluxes. We describe the benchmark models we choose to present in this work and discuss the existing constraints on the couplings for the models in section 3. In section 4, we compute the flux of CRBDM from the knowledge of the fluxes of different cosmic-ray components. We write down the expression for the calculation of event rate in section 5.1. In section 5.2, we constrain the dark-sector coupling using the XENONnT data. We translate the above mentioned bounds to the DM-electron interaction cross section as a function of DM mass for the corresponding models in section 5.3. In section 5.4, we present a rough estimation of the upper bound

---

[1]Many new direct detection ideas with low detection threshold energy have been proposed targeting sub-MeV DM [18–23].

[2]For the impact of the interference between the standard and non-standard neutrino interactions in U(1)-extended models, see ref. [70] where it is shown that the interference can lead to a transition between non-standard interaction models in the energy range relevant to both dark matter and neutrino experiments.
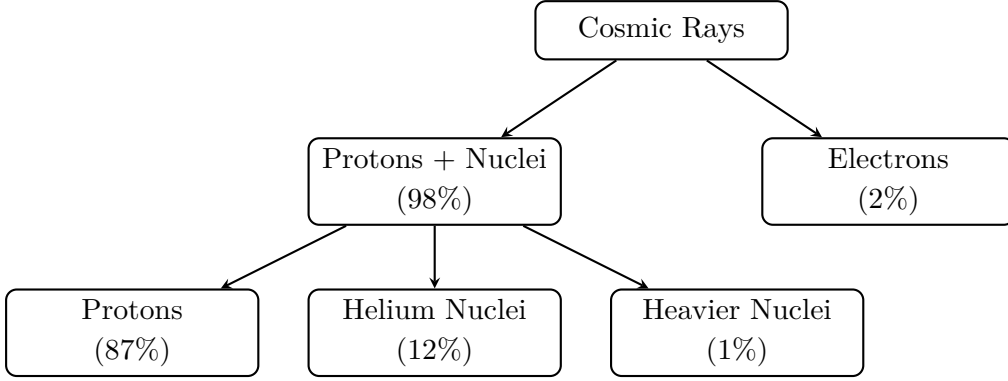
Figure 1. Leading components of cosmic ray and corresponding composition [71].

on the DM-electron interaction cross section due to the shielding effect by the Earth crust. Finally, we conclude in section 6. For additional information, please refer to the appendices, where we include the velocity distribution of CRBDM for some particular parameter sets (appendix A), the comparison of the contributions to the CRBDM fluxes by each individual components of cosmic rays (appendix B), and a simple analytical form for a quick estimation of cross section for the secluded dark-sector model (appendix C).

2   Cosmic rays

As per our present understanding, cosmic rays always consist of charged particles. Additionally, we choose the definition of cosmic rays where neutrinos and gamma rays are excluded. Based on the astrophysical origin, we can classify the cosmic rays into primary, secondary, tertiary rays and so on. The particles, which are accelerated at astrophysical sources, are defined as primary cosmic rays. Secondary ones consist of the particles produced in interaction between the interstellar gas and primary particles. Further interaction between the interstellar gas and the secondary particles, produce tertiary rays and so on. The composition of cosmic rays near the Earth is inferred from the observations. About 2% of the total observed cosmic rays are electrons and rest are baryonic particles. Among baryonic component, about 87% are free protons, remaining cosmic rays consist of 12% helium nuclei and 1% heavier nuclei [71]. Please refer to figure 1 for an overall picture at a glance. While considering only the primary cosmic-ray particles, among nucleons 74% are free protons and 18% are in bound state inside helium nuclei [65].

For primary nucleons, the intensity is roughly parametrized as

$$I_N(E) \approx 1.8 \times 10^4 \left(\frac{E}{1\,\text{GeV}} \right)^{-\alpha} \frac{\text{nucleons}}{\text{m}^2 \cdot \text{s} \cdot \text{sr} \cdot \text{GeV}} \,, \tag{2.1}$$

where E is the energy-per-nucleon and $\alpha = 2.7$. To get the fluxes of the various components of cosmic ray, we follow refs. [66, 72]. We use the parametrization of these fluxes described in section 2.1 and 2.2 in our further calculations.

	a_0	a_1	a_2	a_3	a_4	a_5
p	94.1	-831	0	16700	-10200	0
He	1.14	0	-118	578	0	-87

	b	c	d_1	d_2	e_1	e_2	f_1	f_2	g
p	10800	8590	-4230000	3190	274000	17.4	-39400	0.464	0
He	3120	-5530	3370	1.29	134000	88.5	-1170000	861	0.03

Table 1. Parameters of the analytical fit of the local interstellar proton and Helium spectrum.

2.1 Cosmic-ray electron flux

The cosmic-ray electron flux can be described by certain parametrization of the local interstellar spectrum [72], given as

$$\frac{d\Phi_e}{dT_e}(T_e) = \begin{cases} \dfrac{1.799\times10^{44}\ T_e^{-12.061}}{1+2.762\times10^{36}\ T_e^{-9.269}+3.853\times10^{40}\ T_e^{-10.697}} & \text{for } T_e < 6880\,\text{MeV}\,, \\[1.5em] 3.259\times10^{10}\ T_e^{-3.505} + 3.204\times10^5\ T_e^{-2.620} & \text{for } T_e \geqslant 6880\,\text{MeV}\,, \end{cases} \tag{2.2}$$

where $\frac{d\Phi_e}{dT_e}(T_e)$ is given in $\left(\text{m}^2\cdot\text{s}\cdot\text{sr}\cdot\text{MeV}\right)^{-1}$ and the kinetic energy of the cosmic-ray electrons (T_e) is in MeV. The above parametrization is in accordance with the data from Fermi-LAT [73–76], AMS-02 [77], PAMELA [78, 79], and Voyager [80, 81].

2.2 Cosmic-ray proton and helium fluxes

To estimate the cosmic-ray proton and helium fluxes, we follow refs. [82, 83] and use their analytical form of the functional dependence of the local interstellar proton and helium spectrum on rigidity (R). The differential intensity in terms of rigidity is given by

$$\frac{dI}{dR} \times R^{2.7} = \begin{cases} \sum_{i=0}^{5} a_i R^i & \text{for } R \leqslant 1\ \text{GV}\,, \\[1.5em] b + \dfrac{c}{R} + \dfrac{d_1}{d_2+R} + \dfrac{e_1}{e_2+R} + \dfrac{f_1}{f_2+R} + gR & \text{for } R > 1\ \text{GV}\,, \end{cases} \tag{2.3}$$

where the parameter set are given in table 1. The cosmic-ray proton and Helium fluxes are then obtained by the following relations

$$\begin{aligned} \frac{d\Phi_p}{dT_p}(T_p) &= 4\pi \frac{dR}{dT_p}\frac{dI}{dR}\,, \\ \frac{d\Phi_{He}}{dT_{He}}(T_{He}) &= 4\pi \frac{dR}{dT_{He}}\frac{dI}{dR}\,. \end{aligned} \tag{2.4}$$

These analytical forms of the fluxes stated above are useful in our analysis where DM is boosted by the electrons and/or nucleus depending on the model considered. We choose to work on the models described in section 3.1. Based on the expressions (eqs. (2.2), (2.3), and (2.4)), we estimate the CRBDM flux in section 4.

3 Models

In this section, we describe the benchmark models to examine in this work and briefly discuss the existing constraints on their model parameters. Our study considers models with an additional $U(1)'$, including the secluded dark photon, $U(1)_{B-L}$, and $U(1)_{L_e-L_\mu}$, to investigate the impact of cosmic-ray components on the CRBDM flux and the energy dependence of the cross section.

3.1 Benchmark models

To provide an extensive analysis, we work on the following benchmark models. The coupling to the SM leptons and/or baryons varies for different models and that yields variations in our final result as we will see in section 5.

- Secluded dark sector (dark photon): We consider a hidden sector with a new $U(1)'$ gauge symmetry (A' being the new gauge boson) and a Dirac fermion χ,

$$\mathcal{L} = \mathcal{L}_{\text{SM}} + \bar{\chi}\left(i\partial\!\!\!/ - m_\chi\right)\chi - g_\chi \bar{\chi}\gamma_\mu \chi \hat{A}'^\mu$$
$$+ \frac{1}{2}m_{\hat{A}'}^2 \hat{A}'_\mu \hat{A}'^\mu - \frac{1}{4}\hat{A}'_{\mu\nu}\hat{A}'^{\mu\nu} - \frac{\sin\varepsilon}{2}\hat{B}_{\mu\nu}\hat{A}'^{\mu\nu}, . \tag{3.1}$$

Here, the additional $U(1)'$ is assumed to be spontaneously broken which yields the mass $m_{\hat{A}'}$. Due to the $U(1)_Y \times U(1)'$ kinetic mixing, the dark photon (A') can couple to the SM fermions [69, 84, 85]. We follow ref. [69] to diagonalize away the kinetic mixing term and get the relevant interaction terms as follows

$$\mathcal{L} \supset A'_\mu \left[g^{A'}_{fL} \ \bar{f}\gamma^\mu P_L f + g^{A'}_{fR} \ \bar{f}\gamma^\mu P_R f + g^{A'}_\chi \ \bar{\chi}\gamma^\mu \chi \right]$$
$$+ Z_\mu \left[g^Z_{fL} \ \bar{f}\gamma^\mu P_L f + g^Z_{fR} \ \bar{f}\gamma^\mu P_R f + g^Z_\chi \ \bar{\chi}\gamma^\mu \chi \right] , \tag{3.2}$$

where f being the SM fermions and the relevant couplings are taken from ref. [69]. In this model, the charged leptons and baryons are coupled to the DM fermion (χ) through the mediator (A') with the coupling strength proportional to the electromagnetic charge at the leading order. In the case of DM-nuclear interaction, the cross section is therefore related to the DM-nucleon cross section by a factor which is proportional to the square of the number of protons inside the corresponding nucleus.

- $U(1)_{B-L}$: The conservation of the difference between the baryon number and the lepton number is described by the new $U(1)'$ gauge symmetry. DM fermions are considered to be charged under the new $U(1)' \equiv U(1)_{B-L}$ and SM fermions are already charged under the new gauge symmetry due to the baryonic and leptonic quantum numbers [86],

$$\mathcal{L}_{B-L} \supset g_{B-L}\left[-\bar{l}\gamma^\mu A'_\mu l + \frac{1}{3}\bar{q}\gamma^\mu A'_\mu q \right] - g_\chi \bar{\chi}\gamma_\mu \chi A'^\mu . \tag{3.3}$$

In this model, all the leptons and the baryons are coupled to the DM fermions (χ) through the mediator (A') via the lepton or baryon number. Thus, in the case of DM-nuclear interaction, the cross section is enhanced from the DM-nucleon cross section by a factor which is proportional to the square of the total number of baryons inside the corresponding nucleus.

- $U(1)_{L_e - L_\mu}$: In the $U(1)_{L_e - L_\mu}$ model, the new $U(1)'$ gauge symmetry stands for the conservation of the difference between the electronic lepton number and the muonic lepton number [86],

$$\mathcal{L}_{L_e - L_\mu} \supset g_L \left[\bar{l}_e \gamma^\mu A'_\mu l_e - \bar{l}_\mu \gamma^\mu A'_\mu l_\mu \right] - g_\chi \bar{\chi} \gamma_\mu \chi A'^\mu . \tag{3.4}$$

In the framework of this model, the DM cannot be boosted by CR protons or helium nuclei.

All of the models stated above are capable of depicting DM-SM interactions through the new $U(1)'$ gauge boson as the mediator. We use the above mentioned models to estimate the CRBDM flux (section 4) and the event rates (section 5.1) at XENONnT in the following discussions.

3.2 Existing constraints on the model parameters

In this subsection, we discuss the various existing constraints on the overall coupling between the DM and SM fermions for different values of the mass of the corresponding mediators. Depending on the masses of the new $U(1)'$ gauge boson and the dark fermions, mainly two kinds of exclusion limits exist in the present literature [86–89].

1. For $m_\chi > m_{A'}/2$, the dominant decay channel is $A' \to e^- e^+$. The branching ratio of $A' \to e^- e^+$ is considered to be unity for obtaining the limits, and the process is termed as the visible decay mode of a dark photon.

2. For $m_\chi < m_{A'}/2$, the dominant decay channel is $A' \to \chi \bar{\chi}$. Now, the branching ratio of $A' \to \chi \bar{\chi}$ is considered to be unity for obtaining the limits, and the process is termed as the invisible decay mode of a dark photon.

3. In literature, the semi-visible channels also exist but those channels are specifically dependent on the model parameters [90].

In our analysis, we initially constrain the coupling parameters between DM and SM particles for the benchmark models mentioned above and subsequently scattering cross sections. To get an overview of the ruled-out region of the parameter space, we show the consolidated version of the strongest existing constraints obtained from different beam-dump and collider experiments (figure 3) along with our results. In the case of the invisible decay scenario, we have collected the exclusion limits from the Super Proton Synchrotron (SPS) experiments (NA64 [91, 92], NA62 [93]), collider experiment (BaBar [94, 95]), and electron beam-dump experiments (E787 and E949 [96]). The strongest exclusion bounds for the visible decay of the dark photon have been gathered from SPS experiments (NA64 [97], NA48 [98], WASA [99]), collider experiments (BESIII [100], Babar [94, 101], LSND [102], HADES [103], KLOE [104–106]), electron beam-dump experiments (E141 [84, 107], E137 [84, 108–110], E774 [111]), proton beam-dump experiments(nu-Cal [112, 113], CHARM [114]), and electron-nucleus fixed target scattering experiments (APEX [115], A1 [116]). For more details, please refer to refs. [86–89] and section 5.2.

4 Boosted dark matter flux

In this section, we estimate the BDM flux while taking into account the potential candidates of cosmic rays as boosting agent of cold DM particles, namely, cosmic-ray electrons, protons, and Helium nuclei. We calculate the CRBDM flux using the knowledge of cosmic-ray electron, proton, and Helium fluxes summarized in section 2.

For the scattering between cosmic ray and DM, the energy transfer to the cold DM from the CR electrons/protons/Helium nuclei is given by [40–42, 50, 51]

$$
T_\chi = T_\chi^{\max} \left(\frac{1 - \cos\theta}{2} \right)
$$

$$
\text{with} \quad T_\chi^{\max} = \frac{(T_i)^2 + 2 T_i m_i}{T_i + (m_i + m_\chi)^2 / (2 m_\chi)} \,,
\tag{4.1}
$$

where T_i is the kinetic energy of the cosmic-ray particle i and θ is the scattering angle at the center of momentum frame. Solving eq. (4.1), we get the minimum required energy of the cosmic-ray particles to produce BDM with a certain amount of kinetic energy T_χ:

$$
T_i^{\min} = \left(\frac{T_\chi}{2} - m_i \right) \left[1 \pm \sqrt{1 + \frac{2 T_\chi \, (m_i + m_\chi)^2}{m_\chi \, (2 m_i - T_\chi)^2}} \right] \,,
\tag{4.2}
$$

where the $+$ and $-$ signs in eq. (4.2) are applicable for $T_\chi > 2 m_i$ and $T_\chi < 2 m_i$, respectively.

Finally, the CRBDM flux takes the form

$$
\frac{d\Phi_\chi}{dT_\chi} = D_{\text{eff}} \times \frac{\rho_\chi^{\text{local}}}{m_\chi} \left[\int_{T_e^{\min}}^{\infty} dT_e \, \frac{d\Phi_e}{dT_e} \, \frac{d\sigma_{\chi e}}{dT_\chi} \right.
$$

$$
+ \int_{T_p^{\min}}^{\infty} dT_p \, \frac{d\Phi_p}{dT_p} \, \frac{d\sigma_{\chi p}}{dT_\chi} G_p^2(2 m_\chi T_\chi)
$$

$$
\left. + \int_{T_{\text{He}}^{\min}}^{\infty} dT_{\text{He}} \, \frac{d\Phi_{\text{He}}}{dT_{\text{He}}} \, \frac{d\sigma_{\chi \text{He}}}{dT_\chi} G_{\text{He}}^2(2 m_\chi T_\chi) \right]
\tag{4.3}
$$

with

$$
\frac{d\sigma_{\chi i}}{dT_\chi} = g_i^{A'\,2} g_\chi^{A'\,2} \frac{2 m_\chi (m_i + T_i)^2 - T_\chi \left\{ (m_i + m_\chi)^2 + 2 m_\chi T_i \right\} + m_\chi T_\chi^2}{4\pi \left(2 m_i T_i + T_i^2 \right) \left(2 m_\chi T_\chi + m_{A'}^2 \right)^2} \quad (i = e, p, \text{He}) \,,
\tag{4.4}
$$

where D_{eff} is an effective distance out to which we take into account CRs as the source of a possible high-velocity tail in the DM velocity distribution, ρ_χ^{local} is the local energy density of DM, G_i be the nucleon electromagnetic form factors. We include this form factor for the hadronic elastic scattering following refs. [40, 117, 118],

$$
G_i \left(q^2 \right) = \left(1 + \frac{q^2}{\Lambda_i^2} \right)^{-2} \,,
\tag{4.5}
$$

where $\Lambda_p = 770 \, \text{MeV}$, $\Lambda_{He} = 410 \, \text{MeV}$, and q is the momentum transfer. We evaluate the BDM fluxes after including this form factor, and do the same calculation after including

the Helm form factor [47]. The obtained fluxes are comparable. In the point-like limit, the differential scattering cross section can be related by

$$\frac{d\sigma_{\chi i}}{d\Omega} = \frac{d\sigma_{\chi i}}{d\Omega}\bigg|_{q^2=0} G_i\left(2m_\chi T_\chi\right) . \tag{4.6}$$

Overall couplings will be a bit different for all three models, and thus for $L_e - L_\mu$ model there will be no contribution from the baryonic sector, i.e., for boosting the DM, proton and helium nuclei will not take part. For different considered models, couplings in eq. (4.4) are as follows.

- Secluded dark sector: $\left|g_e^{A'}\right| = \left|g_p^{A'}\right| = e\varepsilon\cos\theta_W, \left|g_{He}^{A'}\right| = 2\left|g_p^{A'}\right|, g_\chi^{A'} = g_\chi$ with θ_W being the Weinberg angle.

- $U(1)_{B-L}$: $\left|g_e^{A'}\right| = \left|g_p^{A'}\right| = g_{B-L}, \left|g_{He}^{A'}\right| = 4\left|g_p^{A'}\right|, g_\chi^{A'} = g_\chi$.

- $U(1)_{L_e-L_\mu}$: $\left|g_e^{A'}\right| = g_L, g_\chi^{A'} = g_\chi$.

We start with the secluded dark photon model to calculate cosmic-ray electron-boosted DM flux which is in agreement with that in ref. [45]. Then we calculate the boosted DM flux and show it in figure 2 taking all the contributions from cosmic-ray electrons, protons and helium nuclei. In this model, the boost contribution due to the helium nuclei is proportional to the number of protons inside the nucleus. Similar flux estimation has been done for the $U(1)_{B-L}$ model and the $U(1)_{L_e-L_\mu}$ model. For a detailed discussion on the latter models, please refer to appendix B. For the $U(1)_{L_e-L_\mu}$ model, DM gets the boost only from the cosmic-ray electron, whereas for the $U(1)_{B-L}$ model, the boost contributions come from electrons, protons, and helium nuclei. Unlike the secluded dark sector, in the $U(1)_{B-L}$ model, the boost contribution due to the helium nuclei is proportional to the total baryon number of the nucleus. For the secluded dark photon model with a reference parameter set of $g_\chi = 1, \varepsilon = 10^{-6}$, we plot the flux of the CRBDM in figure 2.

There are various interesting features in the CRBDM flux distribution. The interface of the two differently colored regions indicates the CRBDM flux for a particular value of $m_{A'}$ which is denoted by the colorbar. From figure 2, we can find that for each m_χ there is a threshold of $m_{A'}$ such that a fixed m_χ produces identical CRBDM flux distribution irrespective of the value of $m_{A'}$ below the threshold. This phenomenon has been reflected in each panel as gradual squeezing of the particular colored region into a line, as one moves across the panels, i.e., from lower m_χ to higher m_χ. For example, the panels of figure 2 shows the gradual squeezing behaviour of the blue colored region into a line if one moves from $m_\chi = 1\,\text{eV}$ to $m_\chi = 1\,\text{GeV}$. In addition, we note that as m_χ increases the threshold value also increases, e.g., the BDM flux distribution corresponding to $m_{A'} = 10^{-4}$ and $10^{-3}\,\text{MeV}$ is significantly different for $m_\chi = 1\,\text{eV}$ but almost similar for $m_\chi = 1\,\text{keV}$. Analogously, for $m_\chi = 1\,\text{MeV}$ and $1\,\text{GeV}$ the BDM flux distribution becomes independent of $m_{A'}$ when considering $m_{A'} < 10^{-2}\,\text{MeV}$ and $1\,\text{MeV}$, respectively. For very high $m_{A'}$, the BDM flux becomes nearly independent of m_χ. In the subsequent section, we will see that these features induce interesting behaviors in exclusion limits as well.
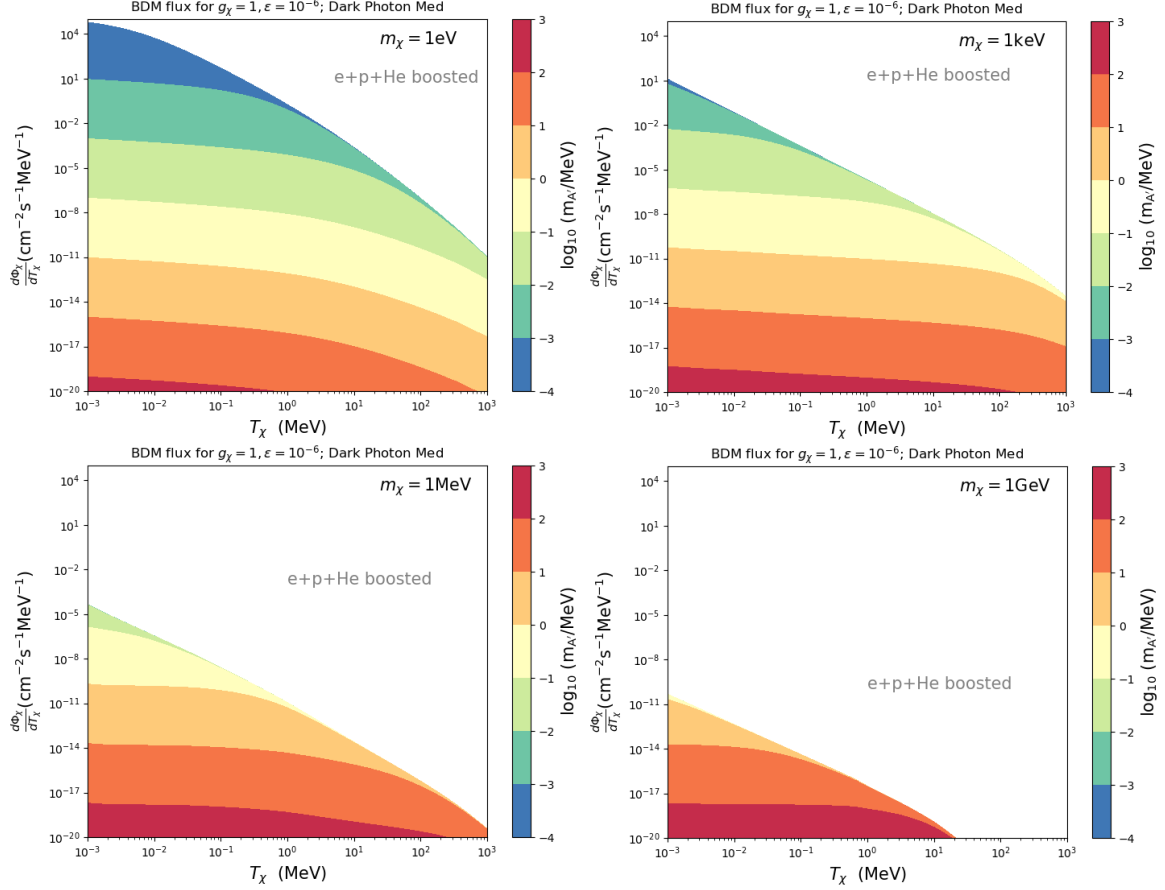
Figure 2. Cosmic-ray electron, proton and Helium nuclei boosted DM flux for the secluded dark photon model with $g_\chi = 1, \varepsilon = 10^{-6}$ and $m_\chi = 1\,\text{eV}, 1\,\text{keV}, 1\,\text{MeV}, 1\,\text{GeV}$, respectively.

5 Results

In this section, we calculate the expected event rate of CRBDM in direct detection experiments. Utilizing the expected event rate and the XENONnT data, we estimate the constraints on the new couplings of the benchmark models which are later translated to the bounds on the DM-electron scattering cross section. In addition, we provide an estimation procedure of the upper bound on the DM-electron interaction cross section due to the Earth shielding effect.

5.1 Differential event rate

With the knowledge of the CRBDM flux discussed in the previous section, we can estimate the differential event rate for the electron recoil spectrum in XENONnT [50, 51, 56],

$$\frac{dR}{dE_R} = \frac{Z_{\text{Xe}}}{m_{\text{Xe}}} \int_{T_\chi^{\min}}^\infty dT_\chi \frac{d\Phi_\chi}{dT_\chi} \frac{d\sigma_{\chi e}}{dE_R} \, , \tag{5.1}$$

where Z_{Xe} is the effective atomic number of xenon and m_{Xe} is the mass of a single xenon atom. Z_{Xe} has been taken as 40 to incorporate the fact that all the xenon atoms are not available for ionization [56].

We do chi-square analysis to obtain the exclusion limits in section 5.2 and the subsequent discussions. In addition, we use a convolution along with the electron recoil spectrum given in eq. (5.1) as suggested by ref. [119], which is basically a Gaussian detector response function with a width given as

$$\sigma(E) = a\sqrt{E} + bE \,, \tag{5.2}$$

where $a = 0.31\sqrt{\text{keV}}$ and $b = 0.0037$.

5.2 Constraints on the coupling

We constrain the overall coupling for all the three models mentioned previously, using the XENONnT electron-recoil data [12].[3] In figure 3, we show the exclusion limit in the coupling vs $m_{A'}$ plane for the scenarios of the invisible and the visible decay of dark photon by setting $g_\chi = 1$. We also show the existing limits for comparison [86]. In ref. [86], the visible decay bounds have small variations for three different models as shown in the right panel of figure 3. For the invisible decay case, we show the existing exclusion limit in magenta. The bounds on the invisible decay of the hidden photon are from NA64 [91, 92], NA62 [93], Babar [94, 95], E787, and E949 [96]. The exclusion limits on the decay of dark photons into the pair of electron-positron (e^+e^-) are from Babar [94, 101], NA64 [97], NA48 [98], E141 [84, 107], E137 [84, 108–110], E774 [111], nu-Cal [112, 113], CHARM [114], KLOE [104–106], WASA [99], HADES [103], APEX [115], A1 [116],BESII [100], and LSND [102]. Our invisible limits in figure 3 correspond to the scenario when there is no provision for the new U(1)$'$ gauge boson (A') to decay into the pair of electron-positron. Depending on the mass of DM (m_χ) and the mass of the new U(1)$'$ gauge boson ($m_{A'}$), A' can or cannot decay into a pair of DM particles ($\chi\bar{\chi}$). The behavior of the exclusion limit plot is consistent with variation of the BDM flux distribution.

As discussed earlier in section 4, there is a threshold of $m_{A'}$ for a given m_χ, below which the CRBDM flux distribution almost is independent of $m_{A'}$, This behavior is reflected to the limits in figure 3. The exclusion limit becomes constant below the threshold of $m_{A'}$ for a fixed m_χ, and the threshold also depends on m_χ as the flux does. On the other hand, above the threshold the BDM flux decreases with increasing $m_{A'}$, and therefore the exclusion limit becomes weaker. For higher $m_{A'}$, the exclusion limit becomes nearly independent of m_χ. Note that only the fluxes for larger than $T_\chi^{\min}$ (from eq. (5.1)) contribute to the event rate and lower m_χ DM is mostly boosted by CR electron as can be seen from appendix B.

In figure 4, we show the exclusion limit for $g_\chi = 1$ in the coupling vs m_χ plane for both of the light and heavy mediator scenarios. We show the exclusion region for all the three models, namely, secluded dark photon, U(1)$_{B-L}$, and U(1)$_{L_e-L_\mu}$. Similar explanation can be drawn for figure 4 using the flux results as done for figure 3. In the left panel, there is a small separation in the exclusion limits at low m_χ for $m_{A'}$=1 eV and 1 keV but at higher m_χ these two limits got merged. This is because for higher m_χ, the BDM flux distributions corresponding to $m_{A'}$=1 eV and 1 keV are identical but at lower m_χ there is a little difference. In the right panel, we can see the exclusion limits tend to become nearly independent of

---

[3]Actually, the limit obtained using XENON1T data [119] is not significantly different from the XENONnT exclusion limit.
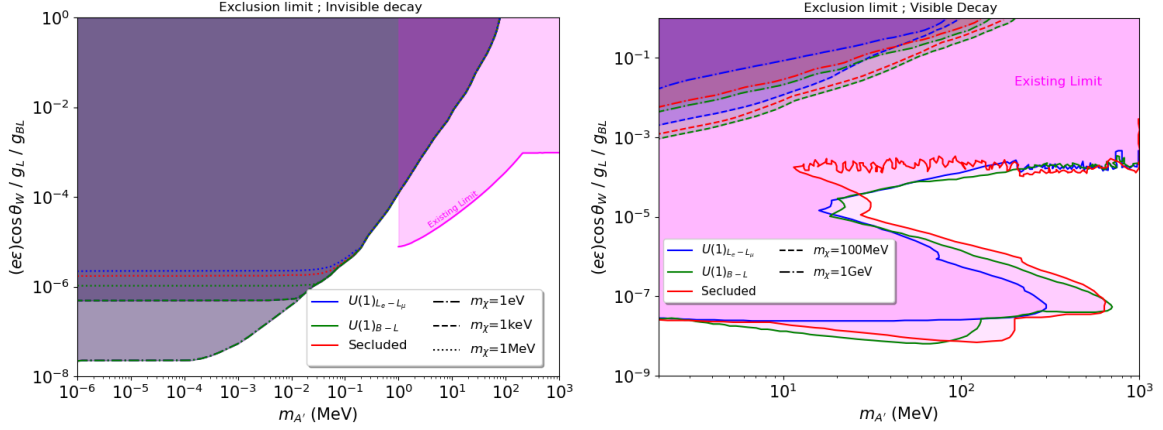
Figure 3. 95% CL exclusion limits from CRBDM in the coupling vs $m_{A'}$ plane: (left) the invisible decay scenario and (right) the visible decay scenario. We compare the three benchmark models for five values of m_χ with $g_\chi = 1$. Shaded regions surrounded by solid lines show existing limits.
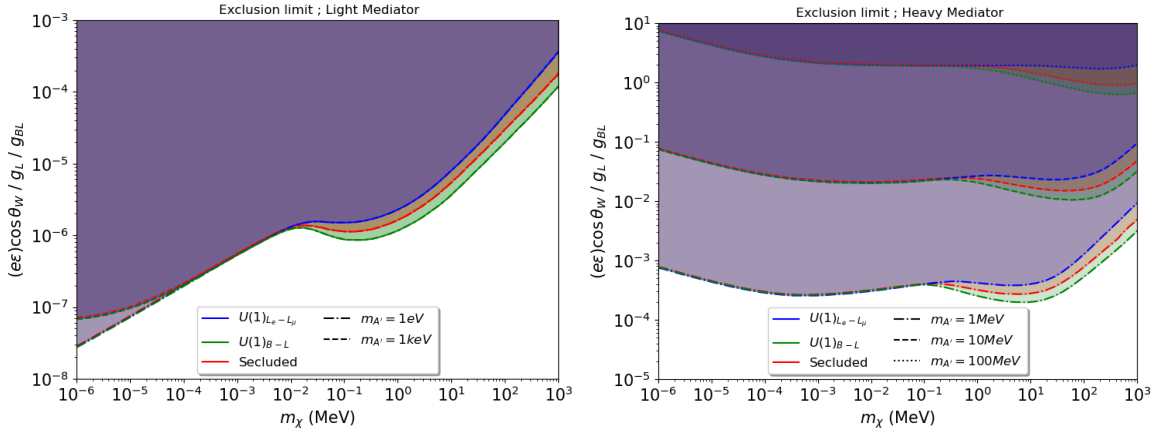

Figure 4. 95% CL exclusion limits in the coupling vs m_χ plane for the three benchmark models and for five values of m_χ with $g_\chi = 1$: (left) the light mediator scenario and (right) the heavy mediator scenario.

m_χ as $m_{A'}$ increases which is consistent with results shown in figure 3. Depending on the mass of the mediator the above mentioned nearly constant lines shifts up or down. For low m_χ, the exclusion limits are same for all of the three benchmark models as the leading contribution comes from CR electron flux; but for higher m_χ, the BDM flux contributions due to proton and helium nuclei become comparable and thus the splittings among limits on different models appear noticeably. The starting point of the splitting depends on $m_{A'}$.

5.3 Constraints on the scattering cross section

Instead of working with energy independent constant cross section, we choose to work on the energy dependent one taking the three benchmark models discussed in section 3. Given a specific model, the differential cross section depends on the DM mass and the kinetic energies of both DM and the electron. Moreover, it depends on the momentum transfer in the collision, and the DM-electron scattering cross section is conventionally normalized

to $\bar{\sigma}_{\chi e}$ with the following definitions [45, 120]:

$$\bar{\sigma}_{\chi e} = \frac{\mu_{\chi e}^2 \, \overline{|\mathcal{M}_{\text{free}}(\alpha m_e)|^2}}{16\pi m_\chi^2 m_e^2} \,, \tag{5.3}$$

$$\overline{|\mathcal{M}_{\text{free}}|^2} = \overline{|\mathcal{M}_{\text{free}}(\alpha m_e)|^2} \times |F_{\text{DM}}(q)|^2 \,, \tag{5.4}$$

where the form factor is given by (at the detector)

$$\left| F_{\text{DM}}\left(q = \sqrt{2m_e E_R}\right) \right|^2 = \frac{(\alpha^2 m_e^2 + m_{A'}^2)^2}{(2m_e E_R + m_{A'}^2)^2}$$
$$\times \frac{2m_e(m_\chi + T_\chi)^2 - E_R\left[(m_\chi + m_e)^2 + 2m_e T_\chi\right] + m_e E_R^2}{2m_e m_\chi^2} \,. \tag{5.5}$$

In the non-relativistic limit $E_R, T_\chi \ll m_e$,

$$|F_{\text{DM}}(q)|^2 = \frac{(\alpha^2 m_e^2 + m_{A'}^2)^2}{(q^2 + m_{A'}^2)^2} \,, \tag{5.6}$$

which is simplified to $|F_{\text{DM}}(q)| = 1$ in the heavy-mediator limit and $|F_{\text{DM}}(q)| \sim \frac{1}{q^2}$ in the light-mediator limit. With these definitions, the normalized DM-electron scattering cross section is estimated as

$$\overline{|\mathcal{M}_{\text{free}}(\alpha m_e)|^2} = \frac{16 g_e^{A'\,2} g_\chi^{A'\,2} m_e^2 m_\chi^2}{(\alpha^2 m_e^2 + m_{A'}^2)^2} \,,$$

$$\bar{\sigma}_{\chi e} = \frac{g_e^{A'\,2} g_\chi^{A'\,2} \mu_{\chi e}^2}{\pi(\alpha^2 m_e^2 + m_{A'}^2)^2} \,,$$

$$\implies \bar{\sigma}_{\chi e} = \begin{cases} \frac{g_e^{A'\,2} g_\chi^{A'\,2} \mu_{\chi e}^2}{\pi(\alpha^2 m_e^2)^2} & \text{for a light mediator,} \\ \frac{g_e^{A'\,2} g_\chi^{A'\,2} \mu_{\chi e}^2}{\pi(m_{A'}^2)^2} & \text{for a heavy mediator.} \end{cases} \tag{5.7}$$

We are now in the position to find the exclusion limit for the DM-electron scattering cross section from the limit for the couplings obtained in section 5.2. Figure 5 shows our exclusion limit for the $\bar{\sigma}_{\chi e}$ as a function m_χ for the light and the heavy mediator scenarios. For comparison, we include the existing direct detection limits as a magenta shaded region, which are taken from SENSEI [15], EDELWEISS [16], PandaX-II [121], XENON100 [122], XENON1T [123], SuperCDMS [14], DAMIC [124], and DarkSide-50 [6]. The parameters that yield the DM relic abundance consistent with the observation are also shown: freeze-in [125–127] for the light mediator scenario and freeze-out [120] for the heavy mediator scenario. To estimate the upper bound in order to take care of the Earth shielding effect, we compute the attenuated flux and find out the value of cross section for which it is significantly low. More details of the Earth shielding effect is discussed in the following section.

Behavior of the exclusion limits on the cross section follows the tendency of the exclusion limits on the coupling. In both the left and the right panels of figure 5, we can see that, for the low m_χ the lower limits for all the three models get merged, but at higher m_χ they get split. This pattern is consistent with figure 4 and follows from the behavior of BDM
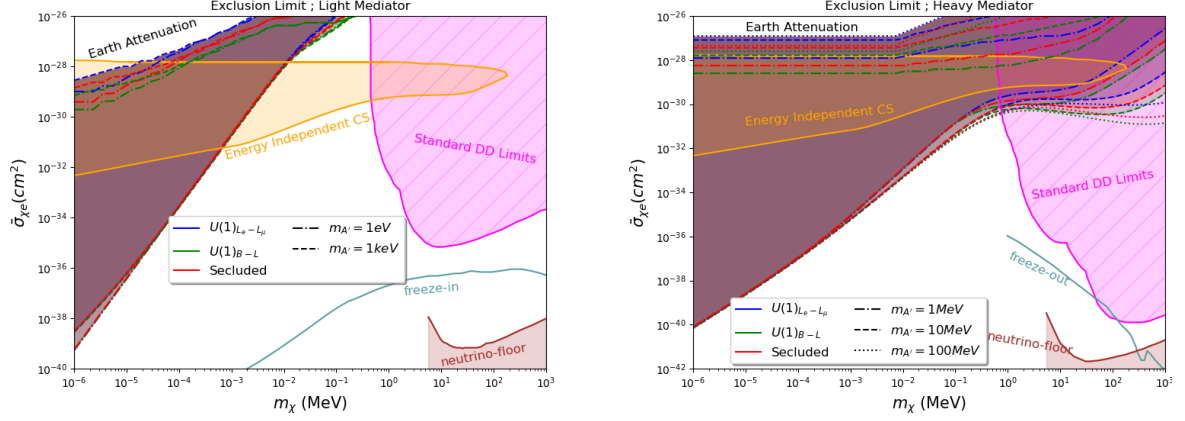
Figure 5. Constraints of DM-electron scattering cross section for $g_\chi = 1$ as a function of m_χ (Left) for the light mediator scenario and (right) the heavy mediator scenario. The limit [51] for constant cross section scenario and the existing direct detection limits are included for comparison. The parameters which provide the observed DM relic abundance are also shown.

flux as discussed in section 5.2. However, the upper limits for all the three models never get merged. This is due to the different Earth shielding effect for the different models caused by the particles present inside the Earth crust; while travelling through the Earth crust towards the detector, BDM interacts only with electrons for the $U(1)_{L_e-L_\mu}$ model, only with the charged particles for the secluded dark photon model, and with all the baryons and leptons for the $U(1)_{B-L}$ model. In addition, we note that the splitting pattern of the lower limit for $m_{A'} = 1\,\text{eV}$ and $m_{A'} = 1\,\text{keV}$ is very similar for figure 4 and figure 5, because for the light mediator the dependence of $\bar{\sigma}_{\chi e}$ on $m_{A'}$ is negligible as seen from eq. (5.7). On the other hand, for the heavy mediator case, the dependence of $\bar{\sigma}_{\chi e}$ on $m_{A'}$ becomes stronger, which causes the lower limits to get merged at low m_χ and only to get split at higher m_χ. This behavior is also consistent with the right panel of figure 4 where it can be seen that the bounds for different $m_{A'}$ are almost parallel for low m_χ and the slopes change only at higher m_χ. The slopes depend on the value of $m_{A'}$; higher the $m_{A'}$, flatter the bound is.

5.4 Attenuation of BDM flux due to the Earth shielding effect

The exact analysis for the upper bound due to the attenuation effect requires monte carlo simulation which is beyond the scope of this work. For an alternative approach, which can give quite good approximate estimation, we basically follow ref. [128]. The kinetic energies of a BDM particle before and after travelling through the Earth to the detector at depth d, are related via the following expression

$$T_\chi^{\text{final}}(d) = T_\chi^{\text{initial}} \exp\left[- \sum_N n_N \frac{2\mu_{\chi N}^2 \sigma_{\chi N}}{m_N m_\chi} d - n_e \frac{2\mu_{\chi e}^2 \sigma_{\chi e}}{m_e m_\chi} d \right], \qquad (5.8)$$

where n_N and n_e are the number densities of nucleus species N and electron in the Earth crust, respectively. For the number densities of the nuclear species, we follow ref. [129].[4] On the

---

[4] $n_N = 2.7\,\text{g/cm}^3 \cdot \text{f}_N \cdot \text{N}_A/\text{A}_N$ where f_N, A_N are the mass fraction and the mass number of the species N and N_A is Avogadro's number.

other hand, we assume a constant number density of the electron, $n_e = 8 \times 10^{23}\,\text{cm}^{-3}$ [41]. The DM-nucleus scattering cross section is related to the DM-nucleon scattering cross section via

$$\sigma_{\chi N} = \begin{cases} \sigma_{\chi n} A_N^2 \frac{\mu_{\chi N}^2}{\mu_{\chi n}^2} & \text{for the } U(1)_{B-L} \text{ model}, \\[3ex] \sigma_{\chi n} Z_N^2 \frac{\mu_{\chi N}^2}{\mu_{\chi n}^2} & \text{for the secluded dark photon model}. \end{cases} \tag{5.9}$$

Then we can estimate the attenuated CRBDM flux by the following expression [40]

$$\frac{d\Phi_\chi}{dT_\chi^{\text{final}}}(d) = \frac{d\Phi_\chi}{dT_\chi^{\text{initial}}}(d=0) \times \frac{dT_\chi^{\text{initial}}}{dT_\chi^{\text{final}}}. \tag{5.10}$$

Here $\frac{d\Phi_\chi}{dT_\chi^{\text{initial}}}$ needs to be evaluated at T_χ^{initial} where T_χ^{initial} along with $\frac{dT_\chi^{\text{initial}}}{dT_\chi^{\text{final}}}$ can be evaluated using eq. (5.8) for any known T_χ^{final}.

We put the modified flux, after considering the attenuation due to Earth scattering, into the event rate equation, eq. (5.1), to evaluate the final differential event rate for electronic recoil. We compute the differential event rate at the detector threshold energy of recoiled electron $\frac{dR}{dE_R}(E_R = E_R^{\text{th}})$ for different values of constant cross section ($\bar{\sigma}_{\chi e}$). Then the attenuation bound (upper limit on $\bar{\sigma}_{\chi e}$) is the value of $\bar{\sigma}_{\chi e}$ above which the CRBDM flux as well as $\frac{dR}{dE_R}(E_R = E_R^{\text{th}})$ become negligible.

The above discussion is a good enough approximation for energy independent cross section consideration and for at most a single scattering scenario. However, the above approach is not directly applicable to our energy-dependent scenario (with multiple scattering). Thus, we need to modify the analysis a bit. Our modified analysis procedure for the attenuation effect is summarized as follows.

- We calculate the average energy transfer per scattering in the Earth crust by the CRBDM particles. The energy transfer in a single scattering as well as the overall cross section in that scattering are dependent on the kinetic energy of the CRBDM before the scattering occurs.

- We fix the final energy of the attenuated CRBDM at the detector depth such that it can produce the electron recoil with recoil energy larger than the lower threshold of the detector. By estimating the average energy transfer and the kinetic energy of CRBDM before the scattering, we calculate the cross section as well as the mean free path.

- If the mean free path is less than the detector depth we redo the analysis by considering the kinetic energy before one scattering as the final energy. At each step, the mean free path is different and dependent on the kinetic energy of CRBDM before scattering.

- We repeat the whole process until the combined mean free path overshoots the detector depth, and from the number of required iterations we obtain the number of scatterings before reaching the detector.

- At the last iteration, we find the initial kinetic energy of CRBDM before entering the Earth crust. Based on the CRBDM flux at the surface, we finally estimate the corresponding flux at the detector depth.

For different normalized cross section, we estimate the final flux and find out the value at which the CRBDM flux drops to a significantly lower value. Those cross sections cause higher number of interactions before reaching the detector, and are thus unable to produce enough recoil to be detected. We set the upper bound by finding out such a value at which the suppression starts.

6 Conclusion

In this work, we examined the cosmic-ray boosted dark matter taking into account the boost due to all the leading components of cosmic rays, namely, electron, proton, and helium nuclei. We computed the flux of CRBDM for three benchmark models: the secluded dark photon, $U(1)_{L_e-L_\mu}$, and $U(1)_{B-L}$. Knowing the flux, we estimated the event rate expected at the XENONnT experiment, and analyzed the exclusion limits on the coupling parameters of the models. Finally, we translated these exclusion limits to the exclusion bounds on the scattering cross section between DM and electron. We also devised a semi-analytic approach to obtain the upper limit on the cross section due to the Earth shielding effect which is an approximate but faster method ever presented in this context. We found that for the dark-matter mass less than $\mathcal{O}(\text{keV})$, the lower exclusion limit with a light mediator is stronger than the limit obtained from the analysis assuming energy independent cross section; the limit with a heavy mediator is stronger than the limit estimated utilizing the energy independent cross section, for most of the DM mass range. Of course, this tendency is dependent on the definition of the normalized cross section; in our work, we estimated the cross section with the conventional value of the momentum transfer in a scattering.

For thermally produced DM, the limit is conventionally drawn down to $1\,\text{keV}$ DM mass because the thermally produced fermionic DM of mass less than $\mathcal{O}(1)\,\text{keV}$ would be hot ($v \gg 10^{-3}c$) and cannot be contained within the galactic halo as a structural part of it. The mass of the fermionic DM is additionally constrained to be $\gtrsim \mathcal{O}(100)\,\text{eV}$ by the Pauli exclusion principle [130]; however, the recent study on ultralight fermionic dark matter [131] shows that the constraint can be relaxed by an order of 16.[5] Thus, although for completeness we consider the light DM down to $1\,\text{eV}$, the validity of fermionic DM of mass less than $\mathcal{O}(1)\,\text{keV}$ is still debatable. Even if we evade the mass constraint following ref. [131], the constraints on the cross section corresponding to low mass DM ($\mathcal{O}(1)\,\text{eV}$) would correspond either to thermally produced hot DM or to non-thermally produced cold DM. In both the cases, the constraints on the cross section will depend on the exact value of ρ_χ which, however, cannot be determined precisely with the current understanding.

Acknowledgments

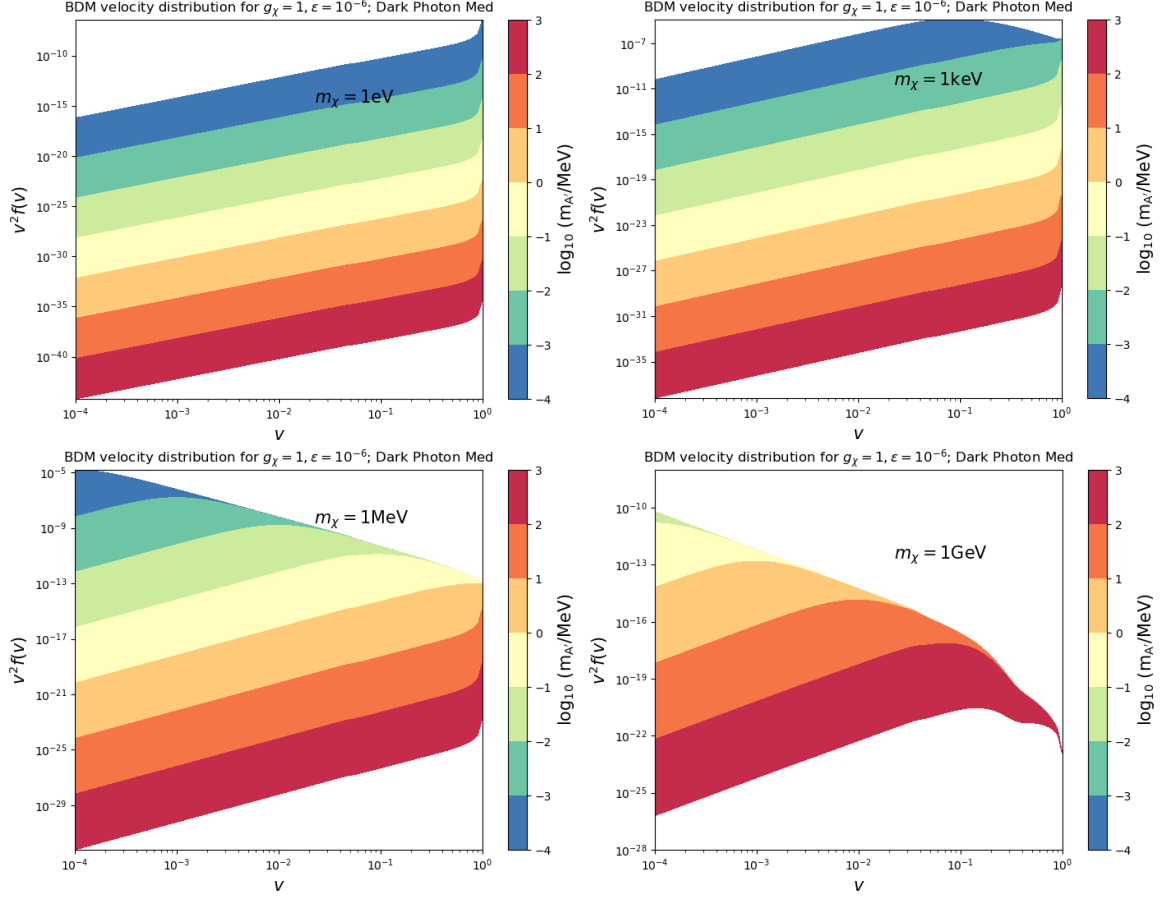[5]For the discussion on the lower bound of bosonic DM mass, see, e.g., ref. [132].

Figure 6. Velocity distribution of CRBDM for $g_\chi = 1, \varepsilon = 10^{-6}$, and $m_\chi = 1\,\text{eV}, 1\,\text{keV}, 1\,\text{MeV}, 1\,\text{GeV}$, respectively.

A   Velocity distribution

We show the velocity distribution of the cosmic-ray boosted dark matter in figure 6 choosing $g_\chi = 1, \varepsilon = 10^{-6}$. To compare with ref. [45], we rewrite eq. (4.4) considering the interaction only with electron as

$$\frac{d\sigma_{\chi e}}{dT_\chi} = \bar{\sigma}_e \frac{\left(\alpha^2 m_e^2 + m_{A'}^2\right)^2}{\mu_{\chi e}^2} \frac{2m_\chi \left(m_e + T_{\text{CR}}\right)^2 - T_\chi \left\{\left(m_e + m_\chi\right)^2 + 2m_\chi T_{\text{CR}}\right\} + m_\chi T_\chi^2}{4\left(2m_e T_{\text{CR}} + T_{\text{CR}}^2\right)\left(2m_\chi T_\chi + m_{A'}^2\right)^2}, \tag{A.1}$$

where α is the electromagnetic fine-structure constant and $\mu_{\chi e}$ is the reduced mass of electron and DM. In addition, the normalized DM-electron scattering cross section is given as

$$\bar{\sigma}_{\chi e} = \frac{\left(g_{eL}^{A'\,2} + g_{eR}^{A'\,2}\right) g_\chi^{A'\,2} \mu_{\chi e}^2}{\pi \left(\alpha^2 m_e^2 + m_{A'}^2\right)^2}. \tag{A.2}$$

Fixing $\bar{\sigma}_{\chi e} = 10^{-30}\,\text{cm}^2$, we obtain the fluxes for CR electron boosted DM as shown in figure 7.

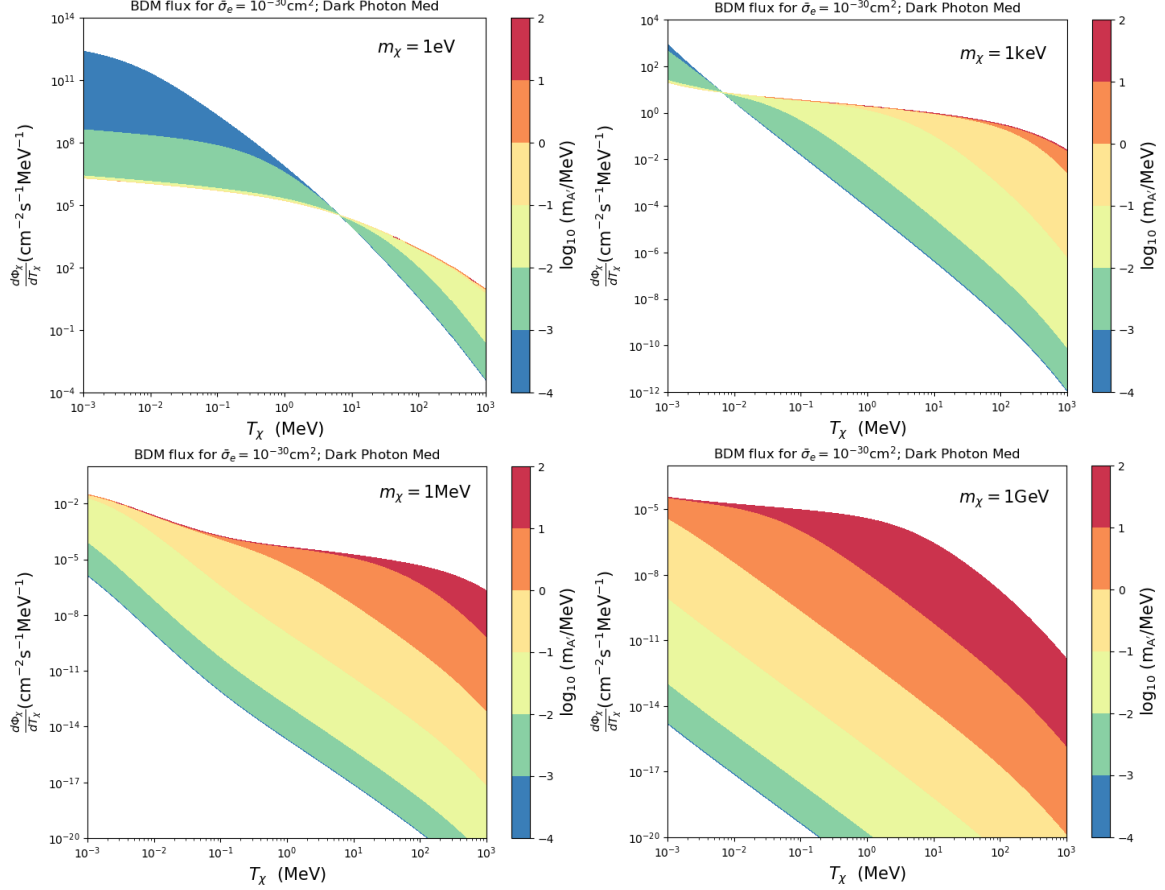**Figure 7.** Cosmic-ray electron boosted DM fluxes for $\bar{\sigma}_e = 10^{-30}\,\mathrm{cm}^2$ and $m_\chi = 1\,\mathrm{eV}$, $1\,\mathrm{keV}$, $1\,\mathrm{MeV}$, $1\,\mathrm{GeV}$, respectively.

B Comparison of BDM fluxes

In figure 8, we separately show the BDM fluxes due to each cosmic-ray species, i.e., electron, proton, and helium for comparison, based on the secluded dark photon model. Similar plots for the $\mathrm{U}(1)_{B-L}$ model and the $L_e - L_\mu$ model are depicted in figure 9 and figure 10, respectively. Note that only cosmic-ray electron boosted DM flux exists for the $L_e - L_\mu$ model.

C Calculation of amplitude and cross section

Here we present a simple analytical form for a quick estimation of cross section for the secluded dark photon model. We follow the relativistic kinematics of two-body scattering process while the second particle is at rest. We obtain eq. (4.1) and thereafter the differential cross section with respect to the kinetic energy [45, 47]

$$\frac{d\cos\theta}{dT_\chi} = -\frac{2}{T_\chi^{\max}},$$

$$\frac{d\sigma_{\chi e}}{dT_\chi} = \frac{d\sigma_{\chi e}}{d\Omega} \cdot \frac{d\Omega}{dT_\chi} = \frac{\overline{|\mathcal{M}|^2}}{16\pi s}\frac{1}{T_\chi^{\max}}. \tag{C.1}$$
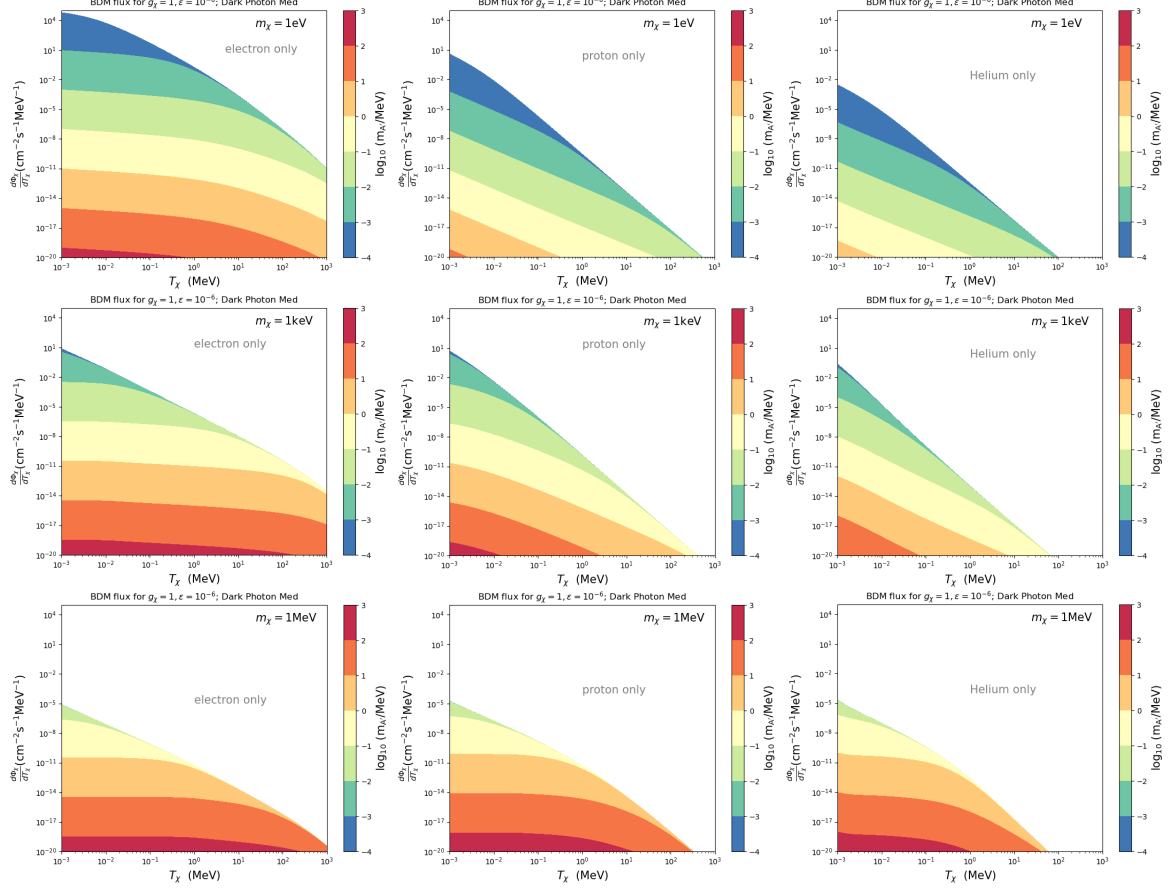
Figure 8. For the secluded dark photon model, cosmic-ray electron (left), proton (middle), and helium (right) boosted DM fluxes for $g_\chi = 1, \varepsilon = 10^{-6}$, and $m_\chi = 1\,\mathrm{eV}, 1\,\mathrm{keV}, 1\,\mathrm{MeV}$, respectively.

The corresponding Mandelstam variables are given by

$$
\begin{aligned}
s &= \left(m_e + m_\chi\right)^2 + 2T_e m_\chi\,, \\
t &= -2m_\chi T_\chi\,, \\
u &= 2\left(m_e^2 + m_\chi^2\right) - s - t\,.
\end{aligned}
\tag{C.2}
$$

The leading contribution of the DM-SM interaction comes from the dark photon mediated channel. However, to take into account the small contributions of the SM Z boson as well, we follow [47]. The complete compact forms are given below.

C.1 DM-electron scattering

For DM-electron interaction, the spin-averaged amplitude square is given by

$$
\begin{aligned}
\overline{|\mathcal{M}|^2} = \frac{2g_\chi^2}{1 - \varepsilon^2} \Bigg[&\left(\frac{s_\xi g_C}{t - m_Z^2} - \frac{c_\xi g_{Cd}}{t - m_{A'}^2}\right)^2 A(m_\chi, m_e) \\
&+ \left(\frac{s_\xi g_A}{t - m_Z^2} - \frac{c_\xi g_{Ad}}{t - m_{A'}^2}\right)^2 B(m_\chi, m_e) \Bigg]\,,
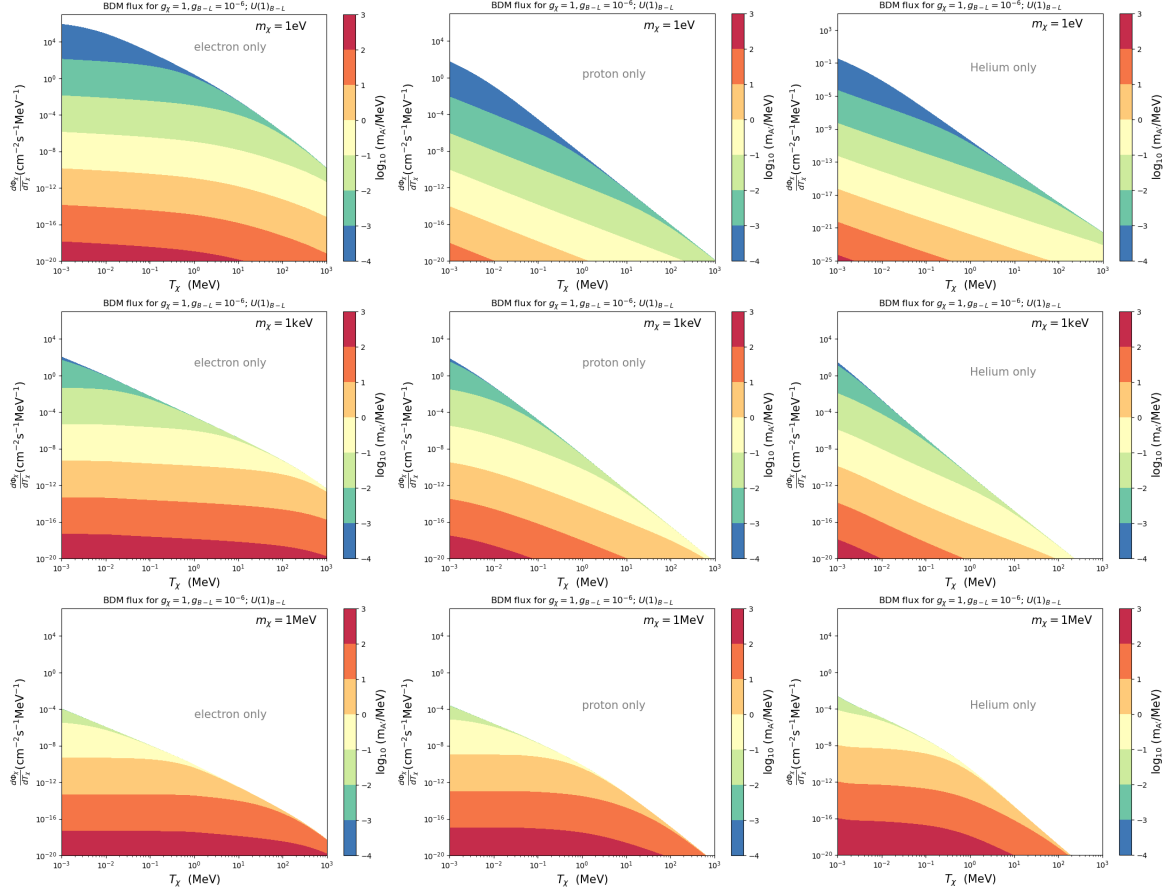\end{aligned}
\tag{C.3}
$$

Figure 9. Cosmic-ray electron (left), proton (middle), and helium (right) boosted DM fluxes for the U(1)$_{B-L}$ model. Others are the same as figure 8.
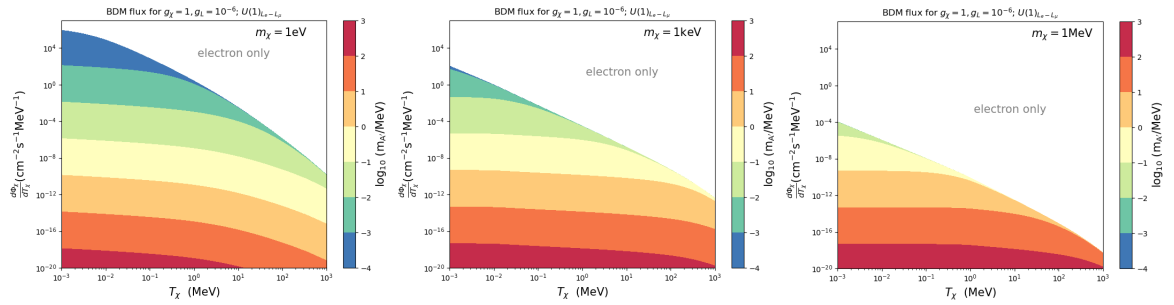

Figure 10. Cosmic-ray electron boosted DM fluxes for the U(1)$_{L_e-L_\mu}$ model. Others are the same as figure 8.

which we have to plug into eq. (C.1) to estimate the differential cross section. Here,

$$g_C = \frac{e}{4}\left[c_\xi\left(3\tan\theta_W - \cot\theta_W\right) + \frac{3s_\xi t_\varepsilon}{c_W}\right],$$

$$g_{Cd} = \frac{e}{4}\left[s_\xi\left(3\tan\theta_W - \cot\theta_W\right) - \frac{3c_\xi t_\varepsilon}{c_W}\right],$$

$$g_A = \frac{e}{4c_W}\left[\frac{c_\xi}{s_W} + s_\xi t_\varepsilon\right],$$

$$g_{Ad} = \frac{e}{4c_W}\left[\frac{s_\xi}{s_W} - c_\xi t_\varepsilon\right], \tag{C.4}$$

and assuming $M^2 = \left(m_\chi^2 + m_i^2\right)$ the functions A, B are given as follows

$$A(m_\chi, m_i) = 2tM^2 + \left(s - M^2\right)^2 + \left(u - M^2\right)^2,$$

$$B(m_\chi, m_i) = \left(s - M^2\right)^2 + \left(u - M^2\right)^2 + 2t\left(m_\chi^2 - m_i^2\right) - 8m_\chi^2 m_i^2. \tag{C.5}$$

C.2 DM-nucleus scattering

For DM-nucleus interaction, the spin-averaged amplitude square is given by

$$\overline{|\mathcal{M}|^2} = \frac{2g_\chi^2}{1-\varepsilon^2}\left[\left(\frac{s_\xi g_{NC}}{t - m_Z^2} - \frac{c_\xi g_{NCd}}{t - m_{A'}^2}\right)^2 A(m_\chi, m_N)\right.$$

$$\left. + \left(\frac{s_\xi g_{NA}}{t - m_Z^2} - \frac{c_\xi g_{NAd}}{t - m_{A'}^2}\right)^2 B(m_\chi, m_N)\right], \tag{C.6}$$

where assuming $M^2 = \left(m_\chi^2 + m_N^2\right)$ the functions A, B are given as

$$A(m_\chi, m_N) = 2tM^2 + \left(s - M^2\right)^2 + \left(u - M^2\right)^2,$$

$$B(m_\chi, m_N) = \left(s - M^2\right)^2 + \left(u - M^2\right)^2 + 2t\left(m_\chi^2 - m_N^2\right) - 8m_\chi^2 m_N^2. \tag{C.7}$$

Again we have to plug this amplitude into eq. (C.1) to estimate the differential cross section. For the nucleus with atomic number Z and mass number A, we have

$$g_{NC} = Zg_C + (A - Z)g_A,$$

$$g_{NCd} = Zg_{Cd} + (A - Z)g_{Ad},$$

$$g_{NA} = (2Z - A)g_A,$$

$$g_{NAd} = (2Z - A)g_{Ad}. \tag{C.8}$$

References

[1] PLANCK collaboration, *Planck 2015 results. XIII. Cosmological parameters*, *Astron. Astrophys.* **594** (2016) A13 [arXiv:1502.01589] [INSPIRE].

[2] G. Bertone, D. Hooper and J. Silk, *Particle dark matter: Evidence, candidates and constraints*, *Phys. Rept.* **405** (2005) 279 [hep-ph/0404175] [INSPIRE].

[3] M.W. Goodman and E. Witten, *Detectability of Certain Dark Matter Candidates*, *Phys. Rev. D* **31** (1985) 3059 [INSPIRE].

[4] DAMA collaboration, *First results from DAMA/LIBRA and the combined results with DAMA/NaI*, *Eur. Phys. J. C* **56** (2008) 333 [arXiv:0804.2741] [INSPIRE].

[5] CRESST collaboration, *Results on light dark matter particles with a low-threshold CRESST-II detector*, *Eur. Phys. J. C* **76** (2016) 25 [arXiv:1509.01515] [INSPIRE].

[6] DARKSIDE collaboration, *Constraints on Sub-GeV Dark-Matter-Electron Scattering from the DarkSide-50 Experiment*, *Phys. Rev. Lett.* **121** (2018) 111303 [arXiv:1802.06998] [INSPIRE].

[7] SUPERCDMS collaboration, *First Dark Matter Constraints from a SuperCDMS Single-Charge Sensitive Detector*, *Phys. Rev. Lett.* **121** (2018) 051301 [*Erratum ibid.* **122** (2019) 069901] [arXiv:1804.10697] [INSPIRE].

[8] XENON collaboration, *First Dark Matter Search with Nuclear Recoils from the XENONnT Experiment*, *Phys. Rev. Lett.* **131** (2023) 041003 [arXiv:2303.14729] [INSPIRE].

[9] LUX collaboration, *Fast and flexible analysis of direct dark matter search data with machine learning*, *Phys. Rev. D* **106** (2022) 072009 [arXiv:2201.05734] [INSPIRE].

[10] PANDAX-4T collaboration, *Dark Matter Search Results from the PandaX-4T Commissioning Run*, *Phys. Rev. Lett.* **127** (2021) 261802 [arXiv:2107.13438] [INSPIRE].

[11] LZ collaboration, *First Dark Matter Search Results from the LUX-ZEPLIN (LZ) Experiment*, *Phys. Rev. Lett.* **131** (2023) 041002 [arXiv:2207.03764] [INSPIRE].

[12] XENON collaboration, *Search for New Physics in Electronic Recoil Data from XENONnT*, *Phys. Rev. Lett.* **129** (2022) 161805 [arXiv:2207.11330] [INSPIRE].

[13] DAMIC-M collaboration, *First Constraints from DAMIC-M on Sub-GeV Dark-Matter Particles Interacting with Electrons*, *Phys. Rev. Lett.* **130** (2023) 171003 [arXiv:2302.02372] [INSPIRE].

[14] SUPERCDMS collaboration, *Constraints on low-mass, relic dark matter candidates from a surface-operated SuperCDMS single-charge sensitive detector*, *Phys. Rev. D* **102** (2020) 091101 [arXiv:2005.14067] [INSPIRE].

[15] SENSEI collaboration, *SENSEI: Direct-Detection Results on sub-GeV Dark Matter from a New Skipper-CCD*, *Phys. Rev. Lett.* **125** (2020) 171802 [arXiv:2004.11378] [INSPIRE].

[16] EDELWEISS collaboration, *First germanium-based constraints on sub-MeV Dark Matter with the EDELWEISS experiment*, *Phys. Rev. Lett.* **125** (2020) 141301 [arXiv:2003.01046] [INSPIRE].

[17] CRESST collaboration, *First results from the CRESST-III low-mass dark matter program*, *Phys. Rev. D* **100** (2019) 102002 [arXiv:1904.00498] [INSPIRE].

[18] Y. Hochberg, Y. Zhao and K.M. Zurek, *Superconducting Detectors for Superlight Dark Matter*, *Phys. Rev. Lett.* **116** (2016) 011301 [arXiv:1504.07237] [INSPIRE].

[19] K. Schutz and K.M. Zurek, *Detectability of Light Dark Matter with Superfluid Helium*, *Phys. Rev. Lett.* **117** (2016) 121302 [arXiv:1604.08206] [INSPIRE].

[20] Y. Hochberg et al., *Detection of sub-MeV Dark Matter with Three-Dimensional Dirac Materials*, *Phys. Rev. D* **97** (2018) 015004 [arXiv:1708.08929] [INSPIRE].

[21] S. Knapen, T. Lin, M. Pyle and K.M. Zurek, *Detection of Light Dark Matter With Optical Phonons in Polar Materials*, *Phys. Lett. B* **785** (2018) 386 [arXiv:1712.06598] [INSPIRE].

[22] Y. Hochberg et al., *Detecting Sub-GeV Dark Matter with Superconducting Nanowires*, *Phys. Rev. Lett.* **123** (2019) 151802 [arXiv:1903.05101] [INSPIRE].

[23] D. Kim, J.-C. Park, K.C. Fong and G.-H. Lee, *Detection of Super-light Dark Matter Using Graphene Sensor*, arXiv:2002.07821 [INSPIRE].

[24] G. Belanger and J.-C. Park, *Assisted freeze-out*, *JCAP* **03** (2012) 038 [arXiv:1112.4491] [INSPIRE].

[25] K. Agashe, Y. Cui, L. Necib and J. Thaler, *(In)direct Detection of Boosted Dark Matter*, *JCAP* **10** (2014) 062 [arXiv:1405.7370] [INSPIRE].

[26] J. Berger, Y. Cui and Y. Zhao, *Detecting Boosted Dark Matter from the Sun with Large Volume Neutrino Detectors*, *JCAP* **02** (2015) 005 [arXiv:1410.2246] [INSPIRE].

[27] K. Kong, G. Mohlabeng and J.-C. Park, *Boosted dark matter signals uplifted with self-interaction*, *Phys. Lett. B* **743** (2015) 256 [arXiv:1411.6632] [INSPIRE].

[28] J.F. Cherry, M.T. Frandsen and I.M. Shoemaker, *Direct Detection Phenomenology in Models Where the Products of Dark Matter Annihilation Interact with Nuclei*, *Phys. Rev. Lett.* **114** (2015) 231303 [arXiv:1501.03166] [INSPIRE].

[29] L. Necib, J. Moon, T. Wongjirad and J.M. Conrad, *Boosted Dark Matter at Neutrino Experiments*, *Phys. Rev. D* **95** (2017) 075018 [arXiv:1610.03486] [INSPIRE].

[30] H. Alhazmi, K. Kong, G. Mohlabeng and J.-C. Park, *Boosted Dark Matter at the Deep Underground Neutrino Experiment*, *JHEP* **04** (2017) 158 [arXiv:1611.09866] [INSPIRE].

[31] D. Kim, J.-C. Park and S. Shin, *Dark Matter "Collider" from Inelastic Boosted Dark Matter*, *Phys. Rev. Lett.* **119** (2017) 161801 [arXiv:1612.06867] [INSPIRE].

[32] G.F. Giudice, D. Kim, J.-C. Park and S. Shin, *Inelastic Boosted Dark Matter at Direct Detection Experiments*, *Phys. Lett. B* **780** (2018) 543 [arXiv:1712.07126] [INSPIRE].

[33] A. Chatterjee et al., *Searching for boosted dark matter at ProtoDUNE*, *Phys. Rev. D* **98** (2018) 075027 [arXiv:1803.03264] [INSPIRE].

[34] D. Kim, K. Kong, J.-C. Park and S. Shin, *Boosted Dark Matter Quarrying at Surface Neutrino Detectors*, *JHEP* **08** (2018) 155 [arXiv:1804.07302] [INSPIRE].

[35] M. Aoki and T. Toma, *Boosted Self-interacting Dark Matter in a Multi-component Dark Matter Model*, *JCAP* **10** (2018) 020 [arXiv:1806.09154] [INSPIRE].

[36] D. Kim, J.-C. Park and S. Shin, *Searching for boosted dark matter via dark-photon bremsstrahlung*, *Phys. Rev. D* **100** (2019) 035033 [arXiv:1903.05087] [INSPIRE].

[37] D. Kim, P.A.N. Machado, J.-C. Park and S. Shin, *Optimizing Energetic Light Dark Matter Searches in Dark Matter and Neutrino Experiments*, *JHEP* **07** (2020) 057 [arXiv:2003.07369] [INSPIRE].

[38] A. De Roeck et al., *Probing Energetic Light Dark Matter with Multi-Particle Tracks Signatures at DUNE*, *JHEP* **11** (2020) 043 [arXiv:2005.08979] [INSPIRE].

[39] H. Alhazmi et al., *Implications of the XENON1T Excess on the Dark Matter Interpretation*, *JHEP* **05** (2021) 055 [arXiv:2006.16252] [INSPIRE].

[40] T. Bringmann and M. Pospelov, *Novel direct detection constraints on light dark matter*, *Phys. Rev. Lett.* **122** (2019) 171801 [arXiv:1810.10543] [INSPIRE].

[41] Y. Ema, F. Sala and R. Sato, *Light Dark Matter at Neutrino Experiments*, *Phys. Rev. Lett.* **122** (2019) 181802 [arXiv:1811.00520] [INSPIRE].

[42] C.V. Cappiello and J.F. Beacom, *Strong New Limits on Light Dark Matter from Neutrino Experiments*, *Phys. Rev. D* **100** (2019) 103011 [*Erratum ibid.* **104** (2021) 069901] [arXiv:1906.11283] [INSPIRE].

[43] J.B. Dent, B. Dutta, J.L. Newstead and I.M. Shoemaker, *Bounds on Cosmic Ray-Boosted Dark Matter in Simplified Models and its Corresponding Neutrino-Floor*, *Phys. Rev. D* **101** (2020) 116007 [arXiv:1907.03782] [INSPIRE].

[44] W. Wang et al., *Cosmic ray boosted sub-GeV gravitationally interacting dark matter in direct detection*, *JHEP* **12** (2020) 072 [*Erratum ibid.* **02** (2021) 052] [arXiv:1912.09904] [INSPIRE].

[45] Q.-H. Cao, R. Ding and Q.-F. Xiang, *Searching for sub-MeV boosted dark matter from xenon electron direct detection*, *Chin. Phys. C* **45** (2021) 045002 [arXiv:2006.12767] [INSPIRE].

[46] Y. Jho, J.-C. Park, S.C. Park and P.-Y. Tseng, *Leptonic New Force and Cosmic-ray Boosted Dark Matter for the XENON1T Excess*, *Phys. Lett. B* **811** (2020) 135863 [arXiv:2006.13910] [INSPIRE].

[47] W. Cho, K.-Y. Choi and S.M. Yoo, *Searching for boosted dark matter mediated by a new gauge boson*, *Phys. Rev. D* **102** (2020) 095010 [arXiv:2007.04555] [INSPIRE].

[48] J.B. Dent et al., *Present and future status of light dark matter models from cosmic-ray electron upscattering*, *Phys. Rev. D* **103** (2021) 095015 [arXiv:2010.09749] [INSPIRE].

[49] C. Xia, Y.-H. Xu and Y.-F. Zhou, *Production and attenuation of cosmic-ray boosted dark matter*, *JCAP* **02** (2022) 028 [arXiv:2111.05559] [INSPIRE].

[50] D. Ghosh, A. Guha and D. Sachdeva, *Exclusion limits on dark matter-neutrino scattering cross section*, *Phys. Rev. D* **105** (2022) 103029 [arXiv:2110.00025] [INSPIRE].

[51] D. Bardhan et al., *Bounds on boosted dark matter from direct detection: The role of energy-dependent cross sections*, *Phys. Rev. D* **107** (2023) 015010 [arXiv:2208.09405] [INSPIRE].

[52] J. Alvey, T. Bringmann and H. Kolesova, *No room to hide: implications of cosmic-ray upscattering for GeV-scale dark matter*, *JHEP* **01** (2023) 123 [arXiv:2209.03360] [INSPIRE].

[53] T.N. Maity and R. Laha, *Cosmic-ray boosted dark matter in Xe-based direct detection experiments*, *Eur. Phys. J. C* **84** (2024) 117 [arXiv:2210.01815] [INSPIRE].

[54] N.F. Bell, J.L. Newstead and I. Shaukat-Ali, *Cosmic-ray boosted dark matter confronted by constraints on new light mediators*, *Phys. Rev. D* **109** (2024) 063034 [arXiv:2309.11003] [INSPIRE].

[55] Y. Jho, J.-C. Park, S.C. Park and P.-Y. Tseng, *Cosmic-Neutrino-Boosted Dark Matter (νBDM)*, arXiv:2101.11262 [INSPIRE].

[56] A. Das and M. Sen, *Boosted dark matter from diffuse supernova neutrinos*, *Phys. Rev. D* **104** (2021) 075029 [arXiv:2104.00027] [INSPIRE].

[57] W. Chao, T. Li and J. Liao, *Connecting Primordial Black Hole to boosted sub-GeV Dark Matter through neutrino*, arXiv:2108.05608 [INSPIRE].

[58] Y.-H. Lin, W.-H. Wu, M.-R. Wu and H.T.-K. Wong, *Searching for Afterglow: Light Dark Matter Boosted by Supernova Neutrinos*, *Phys. Rev. Lett.* **130** (2023) 111002 [arXiv:2206.06864] [INSPIRE].

[59] V. De Romeri, A. Majumdar, D.K. Papoulias and R. Srivastava, *XENONnT and LUX-ZEPLIN constraints on DSNB-boosted dark matter*, *JCAP* **03** (2024) 028 [arXiv:2309.04117] [INSPIRE].

[60] SUPER-KAMIOKANDE collaboration, *Search for Boosted Dark Matter Interacting With Electrons in Super-Kamiokande*, *Phys. Rev. Lett.* **120** (2018) 221301 [arXiv:1711.05278] [INSPIRE].

[61] COSINE-100 collaboration, *First Direct Search for Inelastic Boosted Dark Matter with COSINE-100*, *Phys. Rev. Lett.* **122** (2019) 131802 [arXiv:1811.09344] [INSPIRE].

[62] PANDAX-II collaboration, *Search for Cosmic-Ray Boosted Sub-GeV Dark Matter at the PandaX-II Experiment*, *Phys. Rev. Lett.* **128** (2022) 171801 [arXiv:2112.08957] [INSPIRE].

[63] CDEX collaboration, *Constraints on sub-GeV dark matter boosted by cosmic rays from the CDEX-10 experiment at the China Jinping Underground Laboratory*, *Phys. Rev. D* **106** (2022) 052008 [arXiv:2201.01704] [INSPIRE].

[64] SUPER-KAMIOKANDE collaboration, *Search for Cosmic-Ray Boosted Sub-GeV Dark Matter Using Recoil Protons at Super-Kamiokande*, *Phys. Rev. Lett.* **130** (2023) 031802 [*Erratum ibid.* **131** (2023) 159903] [arXiv:2209.14968] [INSPIRE].

[65] PARTICLE DATA GROUP collaboration, *Review of Particle Physics*, *PTEP* **2022** (2022) 083C01 [INSPIRE].

[66] PARTICLE DATA GROUP collaboration, *Review of Particle Physics*, *Phys. Rev. D* **98** (2018) 030001 [INSPIRE].

[67] J.-H. Huh, J.E. Kim, J.-C. Park and S.C. Park, *Galactic 511 keV line from MeV milli-charged dark matter*, *Phys. Rev. D* **77** (2008) 123503 [arXiv:0711.3528] [INSPIRE].

[68] M. Pospelov, A. Ritz and M.B. Voloshin, *Secluded WIMP Dark Matter*, *Phys. Lett. B* **662** (2008) 53 [arXiv:0711.4866] [INSPIRE].

[69] E.J. Chun, J.-C. Park and S. Scopel, *Dark matter and a new gauge boson through kinetic mixing*, *JHEP* **02** (2011) 100 [arXiv:1011.3300] [INSPIRE].

[70] J.-C. Park and G. Tomar, *Probing non-standard neutrino interactions with interference: insights from dark matter and neutrino experiments*, *JCAP* **08** (2023) 025 [*Erratum ibid.* **02** (2024) E02] [arXiv:2305.10836] [INSPIRE].

[71] M.S. Longair, ed., *High-energy astrophysics. Vol. 1: Particles, photons and their detection*, Cambridge University Press (2011).

[72] M.J. Boschini et al., *HelMod in the works: from direct observations to the local interstellar spectrum of cosmic-ray electrons*, *Astrophys. J.* **854** (2018) 94 [arXiv:1801.04059] [INSPIRE].

[73] FERMI-LAT collaboration, *Measurement of separate cosmic-ray electron and positron spectra with the Fermi Large Area Telescope*, *Phys. Rev. Lett.* **108** (2012) 011103 [arXiv:1109.0521] [INSPIRE].

[74] FERMI-LAT collaboration, *Measurement of the Cosmic Ray e+ plus e- spectrum from 20 GeV to 1 TeV with the Fermi Large Area Telescope*, *Phys. Rev. Lett.* **102** (2009) 181101 [arXiv:0905.0025] [INSPIRE].

[75] FERMI-LAT collaboration, *Fermi LAT observations of cosmic-ray electrons from 7 GeV to 1 TeV*, *Phys. Rev. D* **82** (2010) 092004 [arXiv:1008.3999] [INSPIRE].

[76] FERMI-LAT collaboration, *Cosmic-ray electron-positron spectrum from 7 GeV to 2 TeV with the Fermi Large Area Telescope*, *Phys. Rev. D* **95** (2017) 082007 [arXiv:1704.07195] [INSPIRE].

[77] AMS collaboration, *Precision Measurement of the (e+ + e−) Flux in Primary Cosmic Rays from 0.5 GeV to 1 TeV with the Alpha Magnetic Spectrometer on the International Space Station*, *Phys. Rev. Lett.* **113** (2014) 221102 [INSPIRE].

[78] PAMELA collaboration, *The cosmic-ray electron flux measured by the PAMELA experiment between 1 and 625 GeV*, *Phys. Rev. Lett.* **106** (2011) 201101 [arXiv:1103.2880] [INSPIRE].

[79] CALET collaboration, *Energy Spectrum of Cosmic-Ray Electron and Positron from 10 GeV to 3 TeV Observed with the Calorimetric Electron Telescope on the International Space Station*, *Phys. Rev. Lett.* **119** (2017) 181101 [arXiv:1712.01711] [INSPIRE].

[80] A.C. Cummings et al., *Galactic Cosmic Rays in the Local Interstellar Medium: Voyager 1 Observations and Model Results*, *Astrophys. J.* **831** (2016) 18 [INSPIRE].

[81] E.C. Stone et al., *Voyager 1 Observes Low-Energy Galactic Cosmic Rays in a Region Depleted of Heliospheric Ions*, *Science* **341** (2013) 1236408 [INSPIRE].

[82] M.J. Boschini et al., *Solution of heliospheric propagation: unveiling the local interstellar spectra of cosmic ray species*, *Astrophys. J.* **840** (2017) 115 [arXiv:1704.06337] [INSPIRE].

[83] S. Della Torre et al., *From Observations near the Earth to the Local Interstellar Spectra*, in the proceedings of the *25th European Cosmic Ray Symposium*, Turin, Italy, September 04–09 (2016) [arXiv:1701.02363] [INSPIRE].

[84] M. Fabbrichesi, E. Gabrielli and G. Lanfranchi, *The Dark Photon*, arXiv:2005.01515 [DOI:10.1007/978-3-030-62519-1] [INSPIRE].

[85] P.-H. Gu and X.-G. He, *Electrophilic dark matter with dark photon: from DAMPE to direct detection*, *Phys. Lett. B* **778** (2018) 292 [arXiv:1711.11000] [INSPIRE].

[86] M. Bauer, P. Foldenauer and J. Jaeckel, *Hunting All the Hidden Photons*, *JHEP* **07** (2018) 094 [arXiv:1803.05466] [INSPIRE].

[87] S.C. İnan and A.V. Kisselev, *Search for invisible dark photon in γe scattering at future lepton colliders*, *Eur. Phys. J. C* **82** (2022) 592 [arXiv:2112.13070] [INSPIRE].

[88] A. Filippi and M. De Napoli, *Searching in the dark: the hunt for the dark photon*, *Rev. Phys.* **5** (2020) 100042 [arXiv:2006.04640] [INSPIRE].

[89] S.N. Gninenko, N.V. Krasnikov and V.A. Matveev, *Search for dark sector physics with NA64*, *Phys. Part. Nucl.* **51** (2020) 829 [arXiv:2003.07257] [INSPIRE].

[90] G. Mohlabeng, *Revisiting the dark photon explanation of the muon anomalous magnetic moment*, *Phys. Rev. D* **99** (2019) 115001 [arXiv:1902.05075] [INSPIRE].

[91] Y.M. Andreev et al., *Improved exclusion limit for light dark matter from e^+e^- annihilation in NA64*, *Phys. Rev. D* **104** (2021) L091701 [arXiv:2108.04195] [INSPIRE].

[92] D. Banerjee et al., *Dark matter search in missing energy events with NA64*, *Phys. Rev. Lett.* **123** (2019) 121801 [arXiv:1906.00176] [INSPIRE].

[93] NA62 collaboration, *Search for production of an invisible dark photon in π^0 decays*, *JHEP* **05** (2019) 182 [arXiv:1903.08767] [INSPIRE].

[94] BABAR collaboration, *Dark Photon Studies at BABAR*, *EPJ Web Conf.* **218** (2019) 06001 [INSPIRE].

[95] BaBar collaboration, *Search for Invisible Decays of a Dark Photon Produced in e^+e^- Collisions at BaBar*, *Phys. Rev. Lett.* **119** (2017) 131804 [arXiv:1702.03327] [INSPIRE].

[96] R. Essig et al., *Constraining Light Dark Matter with Low-Energy e^+e^- Colliders*, *JHEP* **11** (2013) 167 [arXiv:1309.5084] [INSPIRE].

[97] NA64 collaboration, *Improved limits on a hypothetical X(16.7) boson and a dark photon decaying into e^+e^- pairs*, *Phys. Rev. D* **101** (2020) 071101 [arXiv:1912.11389] [INSPIRE].

[98] NA48/2 collaboration, *Search for the dark photon in π^0 decays*, *Phys. Lett. B* **746** (2015) 178 [arXiv:1504.00607] [INSPIRE].

[99] WASA-AT-COSY collaboration, *Search for a dark photon in the $\pi^0 \to e^+e^-\gamma$ decay*, *Phys. Lett. B* **726** (2013) 187 [arXiv:1304.0671] [INSPIRE].

[100] BESIII collaboration, *Dark Photon Search in the Mass Range Between 1.5 and 3.4 GeV/c^2*, *Phys. Lett. B* **774** (2017) 252 [arXiv:1705.04265] [INSPIRE].

[101] BaBar collaboration, *Search for a Dark Photon in e^+e^- Collisions at BaBar*, *Phys. Rev. Lett.* **113** (2014) 201801 [arXiv:1406.2980] [INSPIRE].

[102] LSND collaboration, *Evidence for muon-neutrino $\to$ electron-neutrino oscillations from pion decay in flight neutrinos*, *Phys. Rev. C* **58** (1998) 2489 [nucl-ex/9706006] [INSPIRE].

[103] HADES collaboration, *Searching a Dark Photon with HADES*, *Phys. Lett. B* **731** (2014) 265 [arXiv:1311.0216] [INSPIRE].

[104] KLOE-2 collaboration, *Limit on the production of a light vector gauge boson in phi meson decays with the KLOE detector*, *Phys. Lett. B* **720** (2013) 111 [arXiv:1210.3927] [INSPIRE].

[105] KLOE-2 collaboration, *Search for light vector boson production in $e^+e^- \to \mu^+\mu^-\gamma$ interactions with the KLOE experiment*, *Phys. Lett. B* **736** (2014) 459 [arXiv:1404.7772] [INSPIRE].

[106] A. Anastasi et al., *Limit on the production of a low-mass vector boson in $e^+e^- \to U\gamma$, $U \to e^+e^-$ with the KLOE experiment*, *Phys. Lett. B* **750** (2015) 633 [arXiv:1509.00740] [INSPIRE].

[107] E.M. Riordan et al., *A Search for Short Lived Axions in an Electron Beam Dump Experiment*, *Phys. Rev. Lett.* **59** (1987) 755 [INSPIRE].

[108] J.D. Bjorken et al., *Search for Neutral Metastable Penetrating Particles Produced in the SLAC Beam Dump*, *Phys. Rev. D* **38** (1988) 3375 [INSPIRE].

[109] B. Batell, R. Essig and Z. Surujon, *Strong Constraints on Sub-GeV Dark Sectors from SLAC Beam Dump E137*, *Phys. Rev. Lett.* **113** (2014) 171802 [arXiv:1406.2698] [INSPIRE].

[110] L. Marsicano et al., *Dark photon production through positron annihilation in beam-dump experiments*, *Phys. Rev. D* **98** (2018) 015031 [arXiv:1802.03794] [INSPIRE].

[111] A. Bross et al., *A Search for Shortlived Particles Produced in an Electron Beam Dump*, *Phys. Rev. Lett.* **67** (1991) 2942 [INSPIRE].

[112] J. Blümlein and J. Brunner, *New Exclusion Limits for Dark Gauge Forces from Beam-Dump Data*, *Phys. Lett. B* **701** (2011) 155 [arXiv:1104.2747] [INSPIRE].

[113] J. Blümlein and J. Brunner, *New Exclusion Limits on Dark Gauge Forces from Proton Bremsstrahlung in Beam-Dump Data*, *Phys. Lett. B* **731** (2014) 320 [arXiv:1311.3870] [INSPIRE].

[114] S.N. Gninenko, *Constraints on sub-GeV hidden sector gauge bosons from a search for heavy neutrino decays*, *Phys. Lett. B* **713** (2012) 244 [arXiv:1204.3583] [INSPIRE].

[115] APEX collaboration, *Search for a New Gauge Boson in Electron-Nucleus Fixed-Target Scattering by the APEX Experiment*, *Phys. Rev. Lett.* **107** (2011) 191804 [arXiv:1108.2750] [INSPIRE].

[116] H. Merkel et al., *Search at the Mainz Microtron for Light Massive Gauge Bosons Relevant for the Muon g-2 Anomaly*, *Phys. Rev. Lett.* **112** (2014) 221802 [arXiv:1404.5502] [INSPIRE].

[117] C.F. Perdrisat, V. Punjabi and M. Vanderhaeghen, *Nucleon Electromagnetic Form Factors*, *Prog. Part. Nucl. Phys.* **59** (2007) 694 [`hep-ph/0612014`] [ɪɴSPIRE].

[118] Z.-H. Lei, J. Tang and B.-L. Zhang, *Constraints on cosmic-ray boosted dark matter in CDEX-10*, *Chin. Phys. C* **46** (2022) 085103 [`arXiv:2008.07116`] [ɪɴSPIRE].

[119] XENON collaboration, *Excess electronic recoil events in XENON1T*, *Phys. Rev. D* **102** (2020) 072004 [`arXiv:2006.09721`] [ɪɴSPIRE].

[120] R. Essig, J. Mardon and T. Volansky, *Direct Detection of Sub-GeV Dark Matter*, *Phys. Rev. D* **85** (2012) 076007 [`arXiv:1108.5383`] [ɪɴSPIRE].

[121] PᴀɴᴅᴀX-II collaboration, *Search for Light Dark Matter-Electron Scatterings in the PandaX-II Experiment*, *Phys. Rev. Lett.* **126** (2021) 211803 [`arXiv:2101.07479`] [ɪɴSPIRE].

[122] R. Essig, T. Volansky and T.-T. Yu, *New Constraints and Prospects for sub-GeV Dark Matter Scattering off Electrons in Xenon*, *Phys. Rev. D* **96** (2017) 043017 [`arXiv:1703.00910`] [ɪɴSPIRE].

[123] XENON collaboration, *Light Dark Matter Search with Ionization Signals in XENON1T*, *Phys. Rev. Lett.* **123** (2019) 251801 [`arXiv:1907.11485`] [ɪɴSPIRE].

[124] DAMIC collaboration, *Constraints on Light Dark Matter Particles Interacting with Electrons from DAMIC at SNOLAB*, *Phys. Rev. Lett.* **123** (2019) 181802 [`arXiv:1907.12628`] [ɪɴSPIRE].

[125] S.M. Griffin et al., *Multichannel direct detection of light dark matter: Target comparison*, *Phys. Rev. D* **101** (2020) 055004 [`arXiv:1910.10716`] [ɪɴSPIRE].

[126] N. Taufertshöfer, M. Garcia-Sciveres and S.M. Griffin, *Broad-Range Directional Detection of Light Dark Matter in Cryogenic Ice*, `arXiv:2301.04778` [ɪɴSPIRE].

[127] N. Bellomo, K.V. Berghaus and K.K. Boddy, *Impact of freeze-in on dark matter isocurvature*, *JCAP* **11** (2023) 024 [`arXiv:2210.15691`] [ɪɴSPIRE].

[128] T. Emken and C. Kouvaris, *How blind are underground and surface detectors to strongly interacting Dark Matter?*, *Phys. Rev. D* **97** (2018) 115047 [`arXiv:1802.04764`] [ɪɴSPIRE].

[129] T. Emken and C. Kouvaris, *DaMaSCUS: The Impact of Underground Scatterings on Direct Detection of Light Dark Matter*, *JCAP* **10** (2017) 031 [`arXiv:1706.02249`] [ɪɴSPIRE].

[130] S. Tremaine and J.E. Gunn, *Dynamical Role of Light Neutral Leptons in Cosmology*, *Phys. Rev. Lett.* **42** (1979) 407 [ɪɴSPIRE].

[131] H. Davoudiasl, P.B. Denton and D.A. McGady, *Ultralight fermionic dark matter*, *Phys. Rev. D* **103** (2021) 055014 [`arXiv:2008.06505`] [ɪɴSPIRE].

[132] K. Ban et al., *Phenomenological implications on a hidden sector from the festina lente bound*, *PTEP* **2023** (2023) 013B04 [`arXiv:2206.00890`] [ɪɴSPIRE].